ACS OMEGA

Open Access

http://pubs.acs.org/journal/acsodf

Article

An Orthogonal Workflow of Electrochemical, Computational, and Thermodynamic Methods Reveals Limitations of Using a Literature-Reported Insulin Binding Peptide in Biosensors

Katherine Austin,[‖] Jazmine A. Torres,[‖] Jeffery D. V. Waters,[‖] Eva Rose M. Balog, Jeffrey M. Halpern, and Robert J. Pantazes*

Cite This: *ACS Omega* 2024, 9, 39219−39231

Read Online

ACCESS | Metrics & More | Article Recommendations

ABSTRACT: Developing a continuous insulin-monitoring biosensor is of great importance for both the cellular biomanufacturing industry and for treating diabetes mellitus. Such a sensor needs to be able to effectively monitor insulin across a range of temperatures and pHs and with varying concentrations of competing analytes. One of the two main components of any biosensor is the recognition element, which is responsible for interacting with the molecule of interest. Prior literature describes an insulin-binding peptide (IBP) that was reported to bind to insulin with a 3 nM affinity. Here, we used orthogonal and complementary electrochemical, computational, and thermodynamic characterization methods to evaluate IBP's appropriateness for use in a biosensor. Unfortunately, all three methods failed to produce evidence of IBP-insulin binding either on surfaces or in solution. This indicates that the binding exhibited in previous reports is likely restricted to a limited set of conditions and that IBP is not a suitable recognition element for a continuous insulin biosensor.

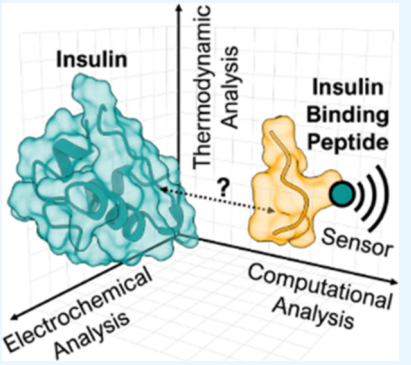

INTRODUCTION

Reliable and convenient detection of insulin holds profound implications for advancing research across diverse domains of human well-being and knowledge. Insulin is a small polypeptide hormone produced by the pancreas that is involved in glucose uptake and metabolism by cells.[1] It is likely most well-known to a general audience for its roles in type 1 diabetes mellitus, caused by insulin deficiency, and type 2 diabetes mellitus, associated with insulin resistance, which are metabolic disorders affecting millions globally.[2,3] Current sensors utilized in diabetes management rely on indirect measurements of glucose, rather than insulin, with continuous glucose monitoring in particular having been shown to improve patient outcomes.[4] Point-of-care continuous monitoring of insulin is expected to further improve outcomes, but progress in developing sensors for this task is still needed.[3,5]

Monitoring insulin levels is also of great importance for biomanufacturing processes. Biomanufacturing is viewed as a critical growth industry in the United States of America. According to a June 25, 2024 White House Fact Sheet, there have been "$29 billion in public and private sector biomanufacturing investments ... since the start of the Biden-Harris Administration" and the administration recently "announced a set of actions to accelerate U.S. domestic biomanufacturing capacity".[6] Cellular biomanufacturing is a major portion of the biomanufacturing industry, and insulin has been shown to be important both to the growth of the cells and to preventing their death in such applications.[7−10] In particular, glucose-stimulated secretion of insulin is a critical quality attribute of pancreatic islet cell therapeutics for the treatment of type 1 diabetes.[11]

Current routine methods for insulin monitoring require sample collection and laboratory testing using techniques such as enzyme-linked immunosorbent assays (ELISA), high-performance liquid chromatography (HPLC), and mass spectrometry.[3] These approaches are time-consuming and expensive; further, the necessity of sample collection for laboratory analysis causes a risk of infection for patients and contamination for biomanufacturing processes.[12] Thus, there is interest in developing novel insulin biosensors for clinical, industrial, and basic research applications.[13−23] For a continuous insulin sensor to be effective for patient care and/or biomanufacturing processes, it must be able to detect insulin under a range of conditions.[3,5] In patients with diabetes, severe ketoacidosis can cause blood pH to drop by a half a logarithmic unit or more from its typical range of 7.35−7.45 to

Received: July 13, 2024
Revised: August 23, 2024
Accepted: August 29, 2024
Published: September 5, 2024

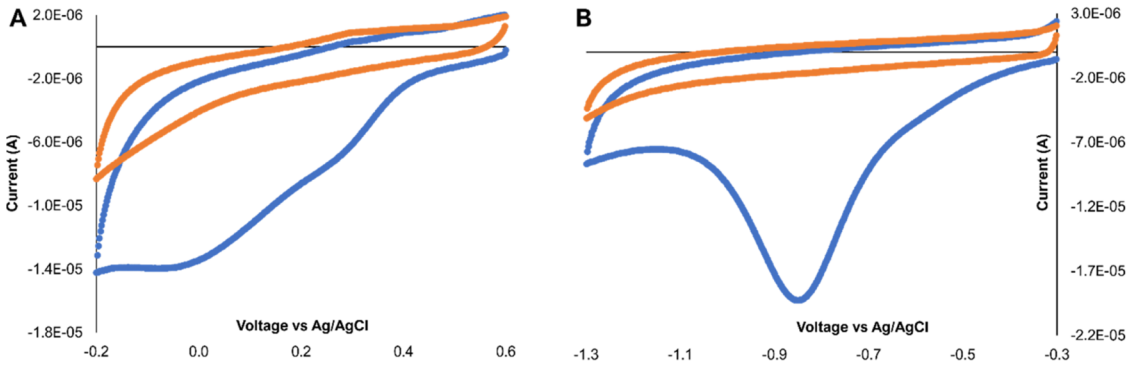

Figure 1. Cyclic voltammetric data indicating (A) the successful attachment of nitrophenyl to the carbon surface and (B) the reduction of nitrophenyl to phenylamine terminal groups. Blue indicates the first scan with a present reduction peak; orange is the second scan with no reduction peak indicating successful attachment.

below 6.9.[24] A patient-worn sensor would also have to work when exposed to varying levels of many protein analytes and small molecules and would experience at least mild temperature changes. Similar challenges occur in any batch-based biomanufacturing process, which have changing media properties over time.

Recognition elements (REs), which bind to target analytes through affinity interactions, are one of the two major components required in biosensors. They produce a measurable signal, which a transducer (i.e., the second component) can interpret into a quantifiable output.[25,26] REs can come in many forms, including aptamers, antibodies, oligomers, enzymes, and peptides.[27] Several electrochemical sensors for insulin have previously been reported. Wu et al. utilized an insulin aptamer and alternating current voltammetry to measure binding to insulin and demonstrated a robust calibration curve.[18] Khanwalker et al. used a single chain variable fragment (i.e., a protein derived from an antibody) and electrochemical impedance spectroscopy (EIS) to a similar end.[28] To our knowledge, a peptide RE has not previously been used in an electrochemical biosensor for insulin, although peptides can have highly specific binding interactions, are inexpensive to produce, and may be more stable under various conditions than other biological REs.[1,29−31]

In 1988, Knutson reported an insulin-binding peptide (IBP) that binds to radiolabeled insulin with a three nanomolar (nM) affinity.[32] IBP is a short sequence of six amino acids (CVEEAS) designed to bind to residues 22−27 of the insulin B-chain. It was designed using the controversial[33] antisense peptide approach, which claims that peptides encoded by complementary sense and antisense nucleic acid sequences are more likely to exhibit specific and high-affinity interactions than randomly selected peptide pairs.[34−37] IBP was one of the first reported high-affinity peptides designed using the antisense method and served as a motivating example for subsequent studies.[38,39] Despite over three decades having passed since the initial publication of IBP, we were able to identify only two reports of the peptide being used. Bisker et al. used IBP as part of a panel of control peptides in an experiment measuring the binding of insulin to polyethylene glycol (PEG) conjugated lipids adsorbed to single-walled carbon nanotubes, although they did not present any data confirming or disconfirming IBP-insulin binding.[40] More recently, Eriksson et al. used IBP with the aim of creating an insulin-binding peptide probe for staining β-cells *in vitro* and *in vivo*.[41] That work demonstrated colocalization of the developed probe with insulin-producing cells through insulin immunostaining but did not directly demonstrate IBP-dependent insulin binding.

There is a significant need for insulin-monitoring sensors and IBP seems like a promising candidate RE due to its strong reported affinity, the colocalization of IBP-bearing probes with insulin-producing cells reported by Eriksson et al., and the general favorable properties of peptides as REs. Yet causes for hesitation about its applicability also exist: there have been no reports since its original publication that directly demonstrate IBP-insulin binding and there was a three-decade gap between the initial literature report and the first example we can find of its use. Despite these possible points of caution, IBP has the potential to function as an RE in an electrochemical sensor. Therefore, IBP is an excellent candidate for our orthogonal electrochemical, computational, and thermodynamic characterization methods for understanding and evaluating protein-peptide binding interactions. Electrochemical characterization in the form of EIS can provide sensitive and quantitative information about analyte binding for sensing applications. Computational characterization using protein docking, energy minimizations, and molecular dynamics (MD) simulations can provide insights into the mechanistic details of how binding events occur. Finally, thermodynamic characterization with isothermal titration calorimetry (ITC) can produce solution-phase binding energies and dissociation constants.

RESULTS AND DISCUSSION

Confirmation of Surface Modification. In order to create an electrochemical sensor, the RE must first be attached to a surface (i.e., carbon electrodes). Functionalization of carbon surfaces occurred in a stepwise process to create an amine terminal surface via diazonium salt chemistry. Carbon electrodes were modified with diazonium salt via electrochemical catalytic reaction. The reduction of the diazonium salt to nitrophenyl carbon surface is observed in Figure 1A; a reduction peak is not observed on the second scan indicating successful attachment. Upon the reduction of nitrophenol to phenylamine, a negative current is observed (Figure 1B) on the first scan indicating successful surface chemistry conversion.

An NHS-ester modified streptavidin was synthesized to link our amine terminated surface with biotinylated RE. The NHS-ester was synthesized in the laboratory and verified through NMR, where peaks shifted from 0.84 and 2.10 (nitrophenol acid) to 0.92 and a cluster of peaks at 1.87 to 2.92 (NHS-ester) (data not shown). The NHS-ester modified streptavidin was

https://doi.org/10.1021/acsomega.4c06481
ACS Omega 2024, 9, 39219−39231

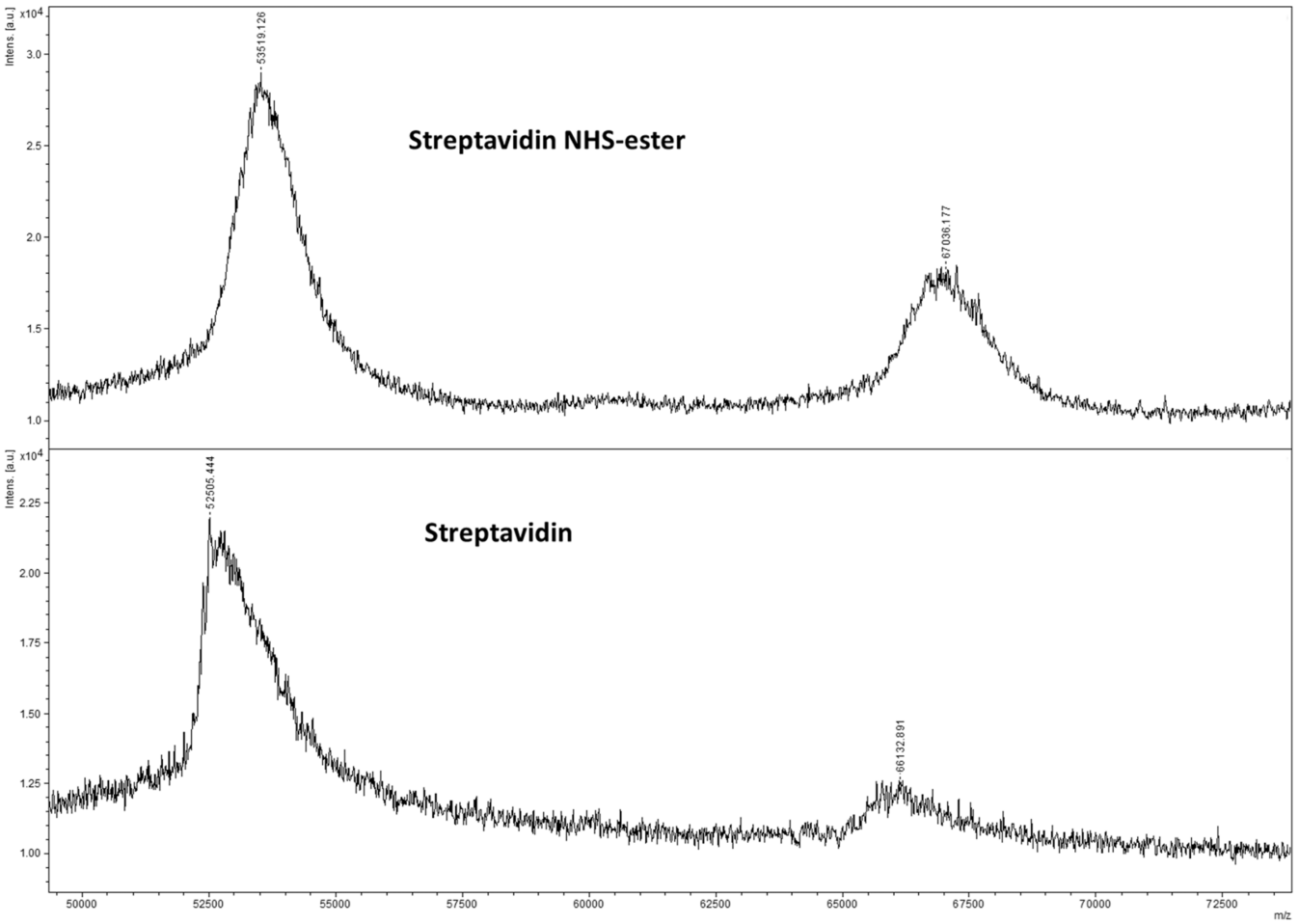

Figure 2. MALDI-TOF Mass Spectrometry Data performed on the purchased streptavidin and the synthesized streptavidin NHS-ester. The data indicate a shift in molecular weight after NHS-ester modification that is consistent with 3−5 NHS-esters attached to each streptavidin molecule.

fabricated in the laboratory and verified with MALDI-TOF mass spectroscopy (Mass Spectroscopy Facility, University of Cincinnati). Figure 2 shows an increase in molecular weight after the streptavidin is successfully modified with the NHS-ester, indicating several NHS-esters modified to each streptavidin molecule (estimated 3−5). The NHS-ester modified streptavidin was used to construct the electrochemical sensor and for the ELISA measurements.

The NHS-ester modified streptavidin was conjugated to the carbon electrode functionalized surface. A biotinylated peptide (IBP-3G-TEV) was added to the surface via the streptavidin/biotin interaction. The conclusion of this surface chemistry should leave an active IBP terminal group allowing IBP-insulin surface binding events to occur.

EIS was used, with 10 mM equimolar (1:1 ratio) of ferricyanide and ferrocyanide, to investigate the different modification stages (Figure 3). A schematic (Figure 3) also demonstrates the terminal groups at each stage where the EIS data was taken. A bare polished electrode has the smallest impedance, demonstrated by the semicircle shape of the graph. The surface terminal group was converted to phenylamine after the electrocatalytic reduction of nitrophenyl to the surface, which shows an increase in the overall impedance. The impedance was further increased after it was exposed and modified to the streptavidin-NHS ester. Finally, the impedance is relatively unchanged when further modified with IBP-3G-TEV via biotin/streptavidin binding. The unchanged impedance in the final stage is not surprising given the small size of IBP-3G-TEV (1.9 kDa) compared to streptavidin (52 kDa).

Surfaces (1)−(4) were further analyzed with ATR-FTIR to verify modification. Figure 4A shows data from a bare electrode subtracted from data for (2) phenylamine, (3) streptavidin, and (4) IBP-3G-TEV. Figure 4B used the (2) phenylamine surface as background to show differences from (3) streptavidin and (4) IBP-3G-TEV surface modifications. The peaks in Figure 4B around 3350 and 1650 cm^{-1} are indicative of successful surface modification with streptavidin. Only subtle differences between the (3) and (4) surfaces were observed, which is consistent with the EIS characterizations of these surfaces. Unfortunately, due to the small size of IBP-3G-TEV compared to streptavidin, it is not possible for us to determine whether the differences in the ATR-FTIR and EIS measurements from surfaces (3) and (4) are due to IBP-3G-TEV attachment or are measurement noise.

Electrochemical Detection of Insulin. We proceeded with electrochemically monitoring insulin binding on the possibly modified IBP-3G-TEV surface by exposing it to increasing concentrations of insulin ranging from 100−400 nM. EIS was taken without a redox mediator, only in the buffered electrolyte, PBS. Although circuit fitting EIS data is a common practice, many applications can also be understood using characteristic features.[42−45] Zphz (or the phase shift of the response) was chosen as a characteristic feature (i.e., a parameter indicative of surface events) due to previous success

https://doi.org/10.1021/acsomega.4c06481
ACS Omega 2024, 9, 39219−39231

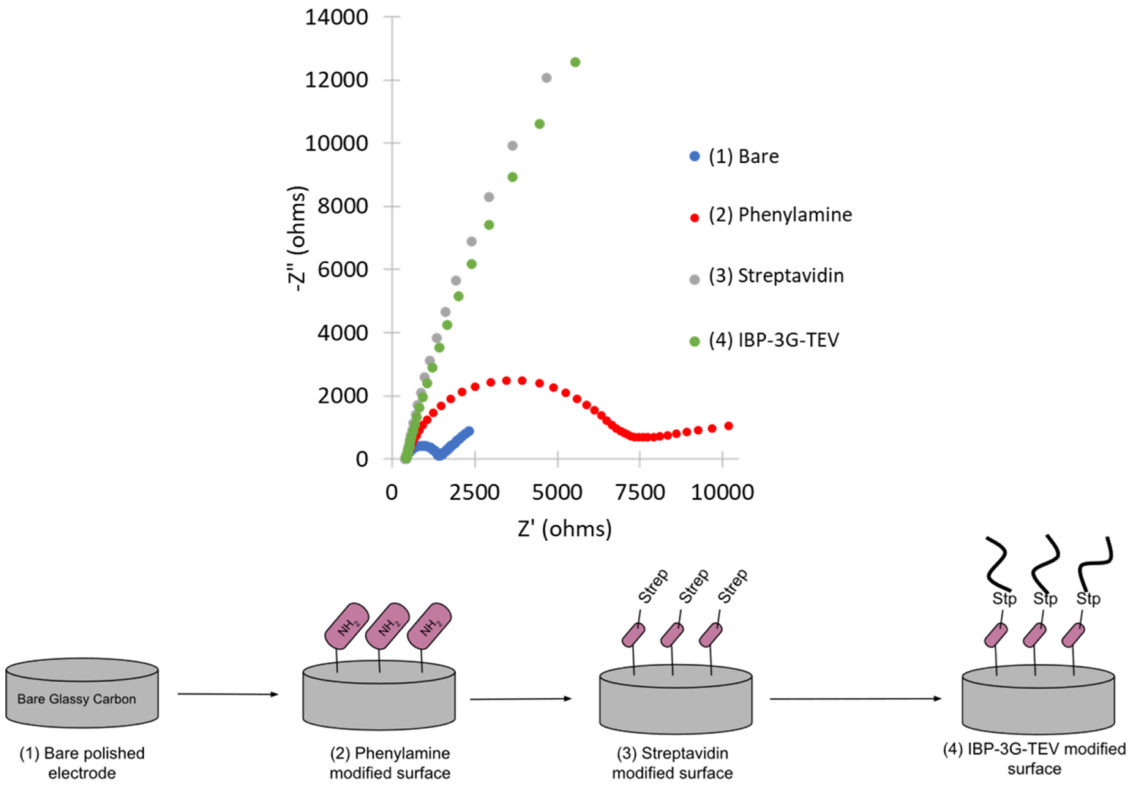

Figure 3. Electrochemical Impedance Spectroscopy Data for Surface Modification Steps. The EIS data was taken in 10 mM ferri/ferrocyanide, to show the progression of surface modification and charge transfer resistance at each stage. The schematic illustrates the corresponding status of surface functionalization at each of the numbered steps in the EIS data.

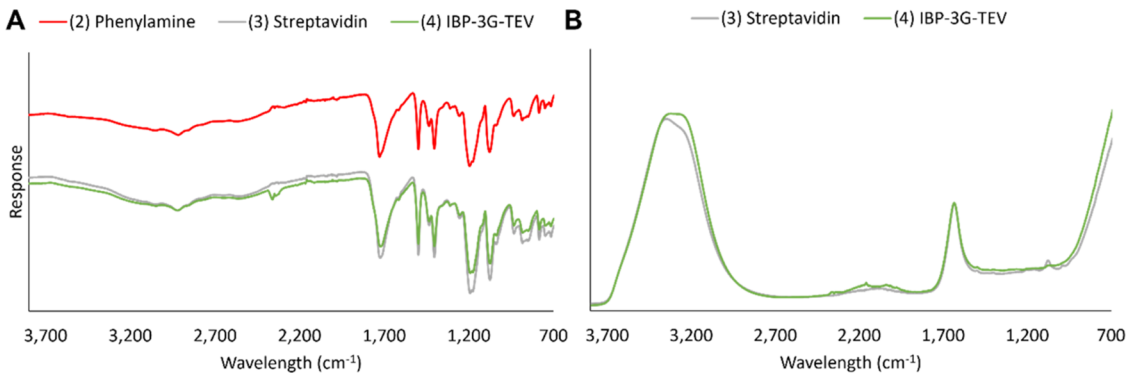

Figure 4. ATR-FTIR data to confirm surface coverage. (A) Bare electrode background subtracted showing the surfaces from Figure 3B (2) phenylamine surface, (3) streptavidin surface, and (4) IBP-3G-TEV surface. (B) The (2) phenylamine surface was subtracted as a background to highlight the changes caused by the (3) streptavidin and (4) IBP-3G-TEV modifications.

in seeing surface changes.[42,46] A scan was taken at 0 nM insulin, or just buffer, for each surface to provide a reference for future scans. Figure 5 shows the phase change difference ($Zphz_0$ - Zphz) at a frequency of 1.00 Hz. The buffer or drift control showed no changes indicating a good choice in feature (Zphz) and frequency (1.00 Hz).

Only one experimental case (IBP surface) responded with insulin concentration, while the other two experimental cases were unresponsive to insulin. This result, of occasional binding between insulin with the modified surface, indicates that the IBP surface may sometimes bind with insulin. However, a scrambled sequence negative control also had one case where it responded to insulin, while the two other cases were unresponsive to insulin. This result, where insulin occasionally binds with the scrambled sequence or the electrochemical surface in general, provides less confidence the IBP recognition element is selective to insulin. Finally, the streptavidin surface (a surface without the added IBP-3G-TEV or the scrambled sequence) also showed a similar response to insulin concentrations compared to the positive-responding IBP case. However, this trend was not observed in all replicas.

Figure 6 shows raw phase change (Zphz) data at multiple frequences for two experimental cases and one scrambled sequence. The largest change across different frequencies is observed in the scrambled sequence negative control compared to the other two experimental cases indicating a potential greater response in the scrambled sequence case. Electrochemical investigation of insulin binding with IBP remains inconclusive, due to the lack of consistent replication and uncertainty regarding whether the surface was successfully

https://doi.org/10.1021/acsomega.4c06481
ACS Omega 2024, 9, 39219−39231

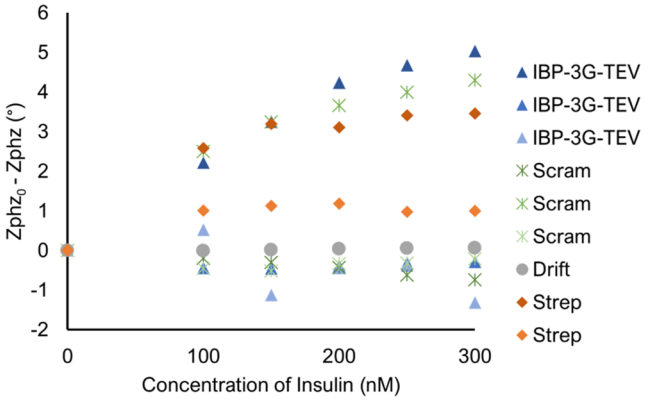

Figure 5. Impedance phase change data versus concentration of insulin for three replicates of the experimental sequence (triangles-blue), three replicates of a scrambled control sequence (cross-green), drift (circle-gray), and streptavidin terminal surface (diamond-orange) at a frequency of 1.00 Hz. One replica each for IBP-3G-TEV, the scrambled negative control sequence, and streptavidin-only surface showed a response, while other replicas did not. Each replica was a new electrode preparation.

modified with IBP-3G-TEV. Therefore, we turned to orthogonal computational and thermodynamic methods to understand and verify the details of this peptide−protein complex.

Computational Analyses. The computational evaluation of IBP began with an all-atom prediction of its binding interactions. No experimentally determined structure of IBP has been previously reported, so a computationally predicted structure was created. As IBP is a peptide with no defined secondary structure, it could potentially bind to insulin in many different conformations. Therefore, a molecular dynamics (MD) simulation of IBP was conducted to generate 1000 possible conformations. The conformations were then clustered into groups of similar structures. Clustering using backbone atoms and a 1.0 Å cutoff yielded 10 clusters, while using all atoms and a 1.5 Å cutoff resulted in 15 identified clusters. The results of clustering are summarized in Table 1. The 25 model structures (i.e., the representative structure from each cluster) were docked to monomeric insulin using ZDOCK,[47] which produced 10 predictions for each structure for a total of 250 putative IBP-insulin complexes. 225 of the 250 complexes positioned the N-terminal C and V of IBP near Y16 and F24 of insulin's B chain, as depicted in Figure 7, which is in proximity to the reported binding site of residues 22−27 of the B chain. The complexes were predicted using global docking and no information about a possible target was provided.

The common recurrence of the N-terminal residues of IBP interacting with that region of insulin in the docking results suggest the presence of features that the docking software

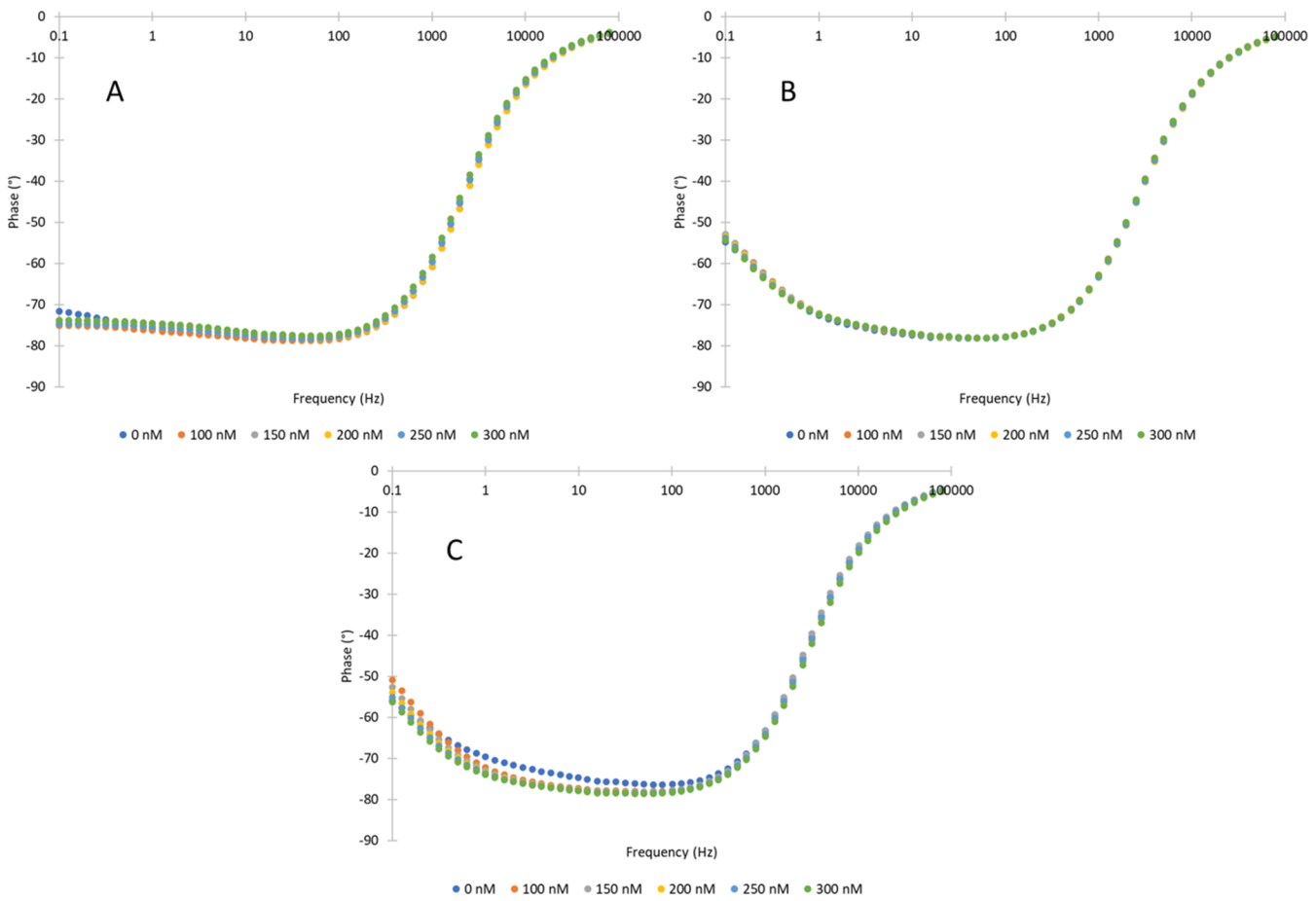

Figure 6. Raw Phase Change Data (A, B) Experimental replicas of exposing the surface to insulin show little variation across different frequencies. (C) is a test case of a scrambled sequence negative control modified surface exposed to different insulin concentrations. The largest change across different frequencies was observed in (C).

https://doi.org/10.1021/acsomega.4c06481
ACS Omega 2024, 9, 39219−39231

Table 1. Sizes and Scores of IBP Structure Clusters[a]

	cluster ID	number of structures	model structure	RMSD score	average RMSD
backbone atom clustering: 1.0 Å cutoff	1	206	396	0.9850	0.6358
	2	179	783	0.9500	0.5946
	3	133	470	0.9790	0.6362
	4	124	990	0.7057	0.4301
	5	111	15	0.9087	0.5690
	6	82	99	0.8345	0.5604
	7	62	224	0.8158	0.5780
	8	47	656	0.9029	0.6627
	9	42	618	0.7968	0.6029
	10	14	610	0.6619	0.5155
all atom clustering: 1.5 Å cutoff	1	223	735	1.4740	0.9894
	2	128	400	1.4621	1.0470
	3	116	385	1.4949	1.1464
	4	113	190	1.3586	0.9793
	5	79	676	1.3375	1.0223
	6	60	489	1.2760	0.9560
	7	58	15	1.4123	0.9957
	8	46	584	1.3551	1.0256
	9	42	158	1.3349	1.0506
	10	40	888	1.1885	0.9158
	11	30	81	1.2675	0.9412
	12	26	633	1.2010	0.9444
	13	19	612	1.3654	0.9787
	14	13	432	1.2031	0.9344
	15	7	653	0.9983	0.7331

[a]The clusters are organized by the number of IBP structures they contain. The model structure of each cluster has an RMSD no worse than the RMSD score for the cluster with every other member of the cluster. The average RMSD values are the mean RMSD of every cluster member with every other cluster member. The structure numbers correspond to the sequential order in which the 1000 IBP conformations were generated during the MD simulation.

views as favorable. The remaining 25 complexes, also shown in Figure 7, do not exhibit any consensus behaviors in their positions. Of the 225 docked complexes that have similar interactions, ones involving the model structures of clusters 3 (385) and 6 (489) of the all-atom clustering results had the strongest Rosetta predicted interaction energies (−23.481 and −24.745 kcal/mol, respectively). It is worth noting that the computationally predicted binding energies are not expected to have experimentally realistic values and that these values are consistent with our expectations based on prior evaluations of complexes of this size. Those two predicted complexes were selected for 100 ns MD simulations to observe their behaviors over time. Figure 8 shows the minimum distances between IBP and insulin during the simulations. IBP stayed in close contact with insulin for portions of both simulations before dissociating and moving far apart. This contrasts with the SH3-Ark1 control complex, which stayed in close contact and had a small RMSD throughout the 100 ns simulation.

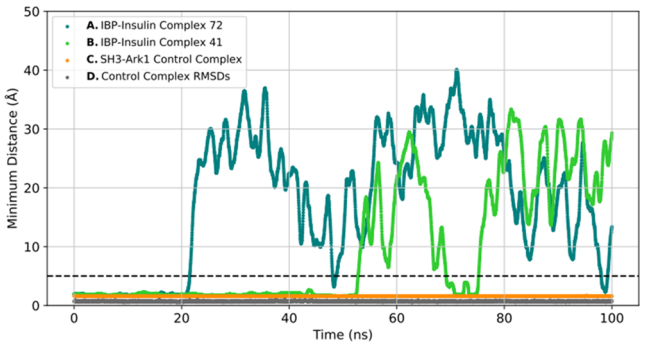

Figure 8. Minimum distance versus time for peptide−protein complexes. The minimum distance between IBP and insulin in the simulated complexes during the 100 ns MD simulations are shown. IBP stayed close to insulin for ∼20 and ∼50 ns in the simulations before dissociating and moving more than 5 Å apart (dashed black line). This contrasts with the SH3-Ark1 control complex, which remained in close contact throughout the 100 ns simulation. The RMSD of the SH3-Ark1 complex is also reported for the control simulation to demonstrate that they not only stayed close to one another but also retained a similar conformation. The minimum distance, but not the RMSD, values have been smoothed by averaging the 10 surrounding points before and after a data point (21 points total) to facilitate the visual interpretation of the data.

The most generous interpretation of these computational results is that they are of mixed quality. It is a promising sign

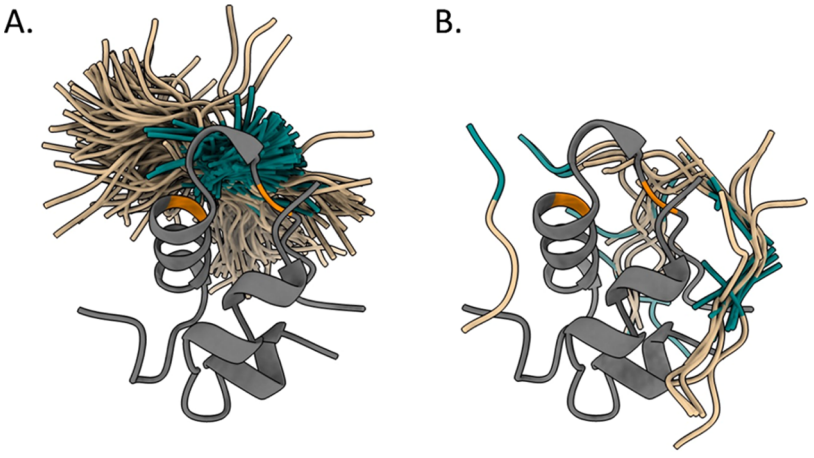

Figure 7. Docking results of IBP with monomeric insulin. 225 of the 250 predicted IBP (tan) - insulin (gray) complexes positioned IBP's N-terminal C and V (green) residues near residues Y16 and F24 (orange) of insulin's B chain, as shown in panel A. F24 in particular is part of the region of residues 22−27 that IBP was designed to bind. Panel B shows the remaining 25 complexes. That many of the docked complexes show similar possible interactions suggest that there is some feature there that the docking program views as especially favorable.

https://doi.org/10.1021/acsomega.4c06481
ACS Omega 2024, 9, 39219−39231

that 225 of 250 predicted docked complexes showed a consensus positioning of the N-terminus of IBP relative to insulin. Further, this area included the region that IBP was reported to bind to insulin (i.e., residues 22−27 on the B chain). When the two complexes with the lowest predicted interaction energies were simulated using 100 ns MD simulations, they both initially showed IBP staying in close contact with insulin before eventual dissociation as the simulations progressed.

A more realistic interpretation of the computational calculations is that they did not produce results that are consistent with binding. Despite recent, well-publicized advances in protein structure prediction driven by machine learning algorithms,[48,49] computationally predicting protein complexes is a challenging problem where favorable false predictions abound. This is exemplified in the data here by the fact that the best of the 25 complexes that did not position IBP near the expected binding site on insulin had a predicted binding energy of −24.027 kcal/mol, which is in between the energies of the two best complexes selected for MD. Our experience is that predictions that look highly promising computationally *might* be experimentally viable while predictions that fail computationally consistently fail experimentally, and the two predicted IBP-insulin complexes here failed to show a lasting binding interaction. That the computational predictions did not produce results consistent with binding is a point of concern but does not preclude the possibility of experimental binding despite our prior experiences. Therefore, we sought to further characterize IBP's binding to insulin using additional experiments.

ELISA. Due to the inconsistent electrochemical and computational data, we performed an ELISA to investigate the binding of an insulin modified surface to IBP. ELISA was performed for all conditions in triplicate with the average and standard deviation of the spectral data shown in Figure 9. A scrambled control was performed to determine specificity of the binding between IBP and insulin.

The formation of disulfide bonds by a peptide sequence can impact its configuration and therefore binding ability, and IBP contains a cysteine residue capable of forming such bonds. Therefore, both the experimental and scrambled conditions were repeated with 3.5 mM TCEP to reduce the formation of disulfide bonds. TCEP was added to the peptide solution prior to the addition of the peptide sequences to the well plates. The addition of TCEP at this step may reduce both false negatives caused by disulfide bond formation between copies of the peptides as well as false positives from disulfide bonds between the peptides and insulin.

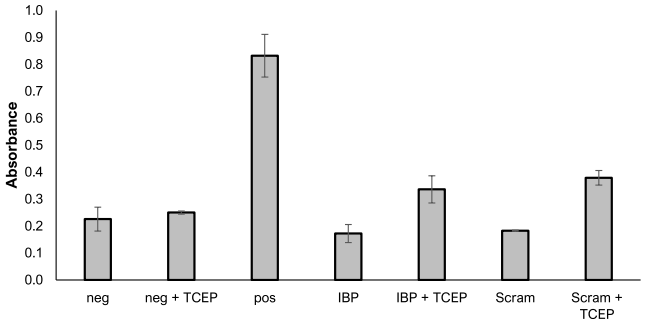

Figure 9. ELISA of (left to right) no insulin negative control, no insulin negative control with IBP-3G-TEV diluted in TCEP, antistreptavidin-HRP positive control, IBP-3G-TEV sequence diluted with UHP, IBP-3G-TEV sequence diluted with TCEP, scrambled sequence diluted with UHP, and scrambled sequence diluted with TCEP. The antistreptavidin-HRP positive control exhibited statistically significantly greater absorbance than the other samples. The data are not consistent with IBP exhibiting specific binding to insulin.

Student's *t* test was performed between the controls and experimental data, with a p-value of less than 0.05 considered statistically significant. Statistical significance was observed between the antistreptavidin-HRP (horseradish peroxidase) positive control and the no insulin negative control, but no statistical significance was observed between the no insulin negative control and experimental sequence data. Conditions with TCEP as a disulfide reducing agent were also not found to be statistically significant compared to the no insulin negative control.

Due to the lack of statistical significance between the no insulin negative control and experimental conditions, it appears there was no binding event between the insulin modified surface and IBP. We confirmed a positive control with a high absorbance (0.83), and our no insulin negative control produced an appropriate low absorbance (0.22). While we observed a difference between IBP and IBP+TCEP (Figure 9), all the experimental cases are not statistically significant above the no insulin negative control. Thus, the experimental and scrambled sequence data leads to the negative conclusion that we did not achieve binding of surface bound insulin with IBP.

ITC. Having been unable to demonstrate IBP-insulin binding either computationally or on surfaces using electrochemistry and ELISA, we attempted to determine the binding affinity of IBP in solution with the minimum possible influence of experimental artifacts using what is considered the gold-standard for quantification of protein−ligand interactions: ITC.[50−52] No detectable binding signal was observed at two different protein−ligand concentrations. Background noise was removed from initial control readings and all heat rates of experimental conditions were corrected using this baseline reading. Figure 10 displays the corrected heat rate and modeling of the titration of 20 μM IBP into 2.5 μM insulin. The heat of mixing in is uniform and consistent, with little to no variation between each injection. Further experimentation yielded similar results. In Figure 10, the graphic displays the corrected heat rate created by the injection of 1 mM IBP into 200 μM insulin. The Q and Fit modeling of the heat rates shows the flat and relatively unchanging heat change between each injection.

CONCLUSIONS

We attempted to validate IBP-insulin binding using orthogonal and complementary electrochemical, computational, and thermodynamic characterization experiments. None of the methods produced results that are indicative of IBP binding with insulin. The computational data included some signs that IBP might bind as intended: 225/250 predicted complexes positioned IBP in proximity to the region of insulin it was designed to bind and the MD-simulated IBP-insulin complexes stayed in close proximity for portions of the simulations. Overall, however, the computational calculations are not consistent with likely IBP-insulin binding. The cause of the lack of binding in the EIS experiments is inconclusive, as it may be due to a failure to modify the surface with IBP-3G-TEV or due to IBP and insulin not binding at the tested conditions. However, that the ELISA (which immobilized insulin on the

https://doi.org/10.1021/acsomega.4c06481
ACS Omega 2024, 9, 39219−39231

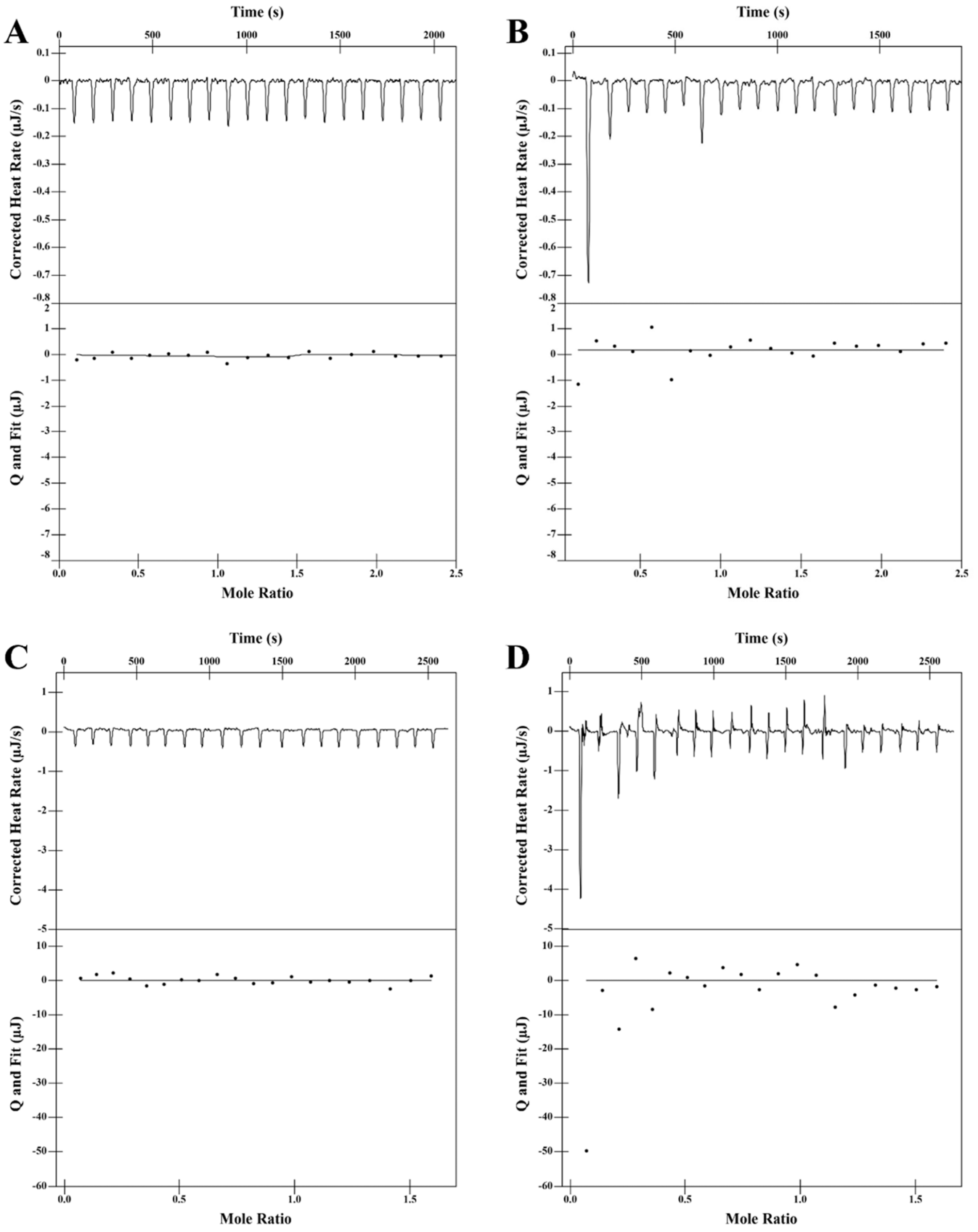

Figure 10. ITC Data. (A) shows the corrected heat rate and modeling of the mixing of 20 μM IBP into 2.5 μM insulin, while (B) depicts the corresponding mixing of control buffer into 2.5 μM insulin. (C) and (D) show the same for mixing 1 mM IBP and control buffer into 200 μM insulin. The heats of mixing are uniform and consistent with minimal if any variation between injections, indicating that no binding of IBP and insulin was detected.

https://doi.org/10.1021/acsomega.4c06481
ACS Omega 2024, 9, 39219−39231

surface, not IBP) and ITC (with both in solution) experiments also could not demonstrate binding suggests that these molecules do not bind at many conditions. We therefore recommend that further investigations of IBP should start by replicating the conditions that Knutson used.

Knutson showed that IBP binds to insulin with a 3 nM affinity, and Ericksson et al. demonstrated that an IBP-conjugated probe colocalized with insulin-producing cells. Those reports indicate that under the right conditions, insulin and IBP can bind. This led us to investigate whether IBP and insulin can bind under other conditions for use in a biosensor. However, we were not able to demonstrate IBP-insulin binding either computationally or experimentally under routine laboratory conditions using a variety of methods, suggesting that the binding interactions require specific conditions. Since a continuous insulin monitoring biosensor necessitates detection of insulin under a wide range of conditions, our findings indicate that IBP is not suitable for use as a RE in such a sensor.

METHODS

Materials. For ELISA and EIS experiments, IBP at a purity ≥95% was ordered from Genscript with a GGG linker and biotinylated C-terminus for surface attachment and termed IBP-3G-TEV (sequence purchased: CVEEASGGGENLYFQ-[Lys(biotin)]). A scrambled IBP sequence control was also ordered from Genscript with a GGG linker and biotinylated C-terminus for surface attachment (sequence purchased: EACVESGGGENLYFQ[Lys(biotin)]). For isothermal titration calorimetry (ITC) experiments, IBP-3G-TEV was ordered from Genscript with ≥95% purity, without the C-terminal Lys or biotinylation (sequence purchased: CVEEASGGGEN-LYFQ). Working (glassy carbon rod) electrode, auxiliary (platinum) electrode, and reference (silver/silver chloride) electrode were obtained from BASinc. A Gamry Reference 600+ potentiostat was used for all electrochemical measurements. Chemicals purchased from Sigma-Aldrich include 99.8% acetonitrile, potassium chloride, 100% hypophosphoric acid, 100% N-N-dimethylformamide, 99.7% acetic acid, 70% nitric acid, 98% sulfuric acid, and high-binding plates. Chemicals purchased from Thermo Fisher scientific include 85% sodium hydrosulfide, 3-(4-hydroxyphenyl)-propionic acid, dichloromethane, Tween-20, SuperBlock blocking buffer in PBS, 98% tris(2-carboxyethyl)-phosphine hydrochloride, streptavidin antibody HRP, tetramethylbenzidine, and commercial blocking buffer. Chemicals purchased from Acros organics include 98% N-hydroxysuccinimide (Sulfo-NHS) and 70% ammonium hydroxide. Both the insulin used for all EIS and ELISA experiments and 98% 4-nitroaniline were purchased from R&D systems. For ITC experiments, recombinant human insulin was purchased from Millipore Sigma. Compressed nitrogen was purchased from Airgas, inc., streptavidin from Invitrogen, and TMB from Life Technologies. Sodium nitrite was purchased from avocado research chemicals, 1H hydrochloric acid at 96.35% from Honeywell, 200 proof ethanol from Pharmco Products, and 98% potassium ferricyanide from Alfa Aesar.

Synthesis of Nitrophenol Streptavidin Complex. 3-(4-hydroxyphenyl)propionic acid was combined with glacial acetic acid in a round-bottom flask in an ice bath at 15 °C. Nitric Acid was added and the solution was stirred for at least 15 min when a color change was observed. The contents of the beaker were poured into 400 mL of ice-cold water to quench the reaction. The solution was vacuum filtered to remove the precipitate which was then transferred to a glass vial and lyophilized overnight. After lyophilization the precipitate was recrystallized by adding a 1:1 ethanol:water solvent heated to 80 °C using a minimal amount to dissolve the entire precipitate. The solution was poured into a flat dish and allowed to cool at room temperature to form crystals. Finally, the solution was again vacuum filtered and dried with the desiccator for at least 6 h to create nitrophenol acid.

Nitrophenol acid was combined with N-hydroxysuccinimide (NHS) in a 1:0.65 ratio in 10 mL dimethyl sulfide in a round-bottom flask. The solution was cooled to approximately 0 °C using an ice bath and stirred for 2 h. The contents of the flask were rinsed twice with ultrahigh purification water (UHP) and once with brine (i.e., saturated NaCl solution). The organic layer was separated and dried with sodium sulfate. Solvent was removed using a vacuum leaving a yellow solid product of NHS-ester.

One mg of streptavidin was solubilized in 100 μL of UHP and transferred to a centrifuge tube. NHS-ester was solubilized with dimethylformamide in the fume hood. Because less than 10% DMF was used in this solution, this process is not expected to impact the structure or binding of streptavidin.[53] 10 μL of the NHS-ester solution was added to the streptavidin solution and allowed to react on a shaker for 2 h. After reacting, the sample was purified by adding it to a 30k MW spin filter and spun at 10,000 rpm for 3 min, and then washed three times with 1X phosphate buffer solution (PBS) at the same centrifuge settings. The contents of the spin filter were transferred to a new centrifuge tube and combined with 10 μL of 10 mM sodium hydrosulfide dissolved in 1X PBS. The tube was shaken for 20 min, washed, and filtered. The final streptavidin-NHS ester product of concentration was verified via NanoDrop.

Surface Modification. *Electrode Polishing.* Carbon electrodes were rinsed with UHP and polished with 0.05 μm alumina slurry polish in a figure eight motion for 2 min, changing direction every 15 s. Electrodes were rinsed again with UHP and dried with compressed nitrogen.

Diazonium Salt Synthesis. 300 μL of 50 mM nitroaniline solution was added to an electrochemical cell containing 15 mL of 4% hydrochloric acid. The electrochemical cell was deoxygenated with compressed nitrogen in an ice bath for 15 min. 300 μL of sodium nitrite were added to the electrochemical cell, covered with parafilm, and placed in an ice bath for 5−10 min.

Creation of Amine-Phenyl Surface. The electrochemical cell was moved to a Faraday cage where the polished carbon electrode was added to the solution as well as the reference and counter electrodes. Cyclic voltammetry was performed at 100 mV/s from 0.6 to −0.2 V vs Ag/AgCl for 2 scans. Working carbon electrode was removed and rinsed thoroughly with UHP. (Note: The diazonium salt solution was quenched at 1:1 ratio with hypophosphorous acid to minimize the risks of this solution).

A solution of 9:1 water:ethanol with 0.1 M potassium chloride was deoxygenated with nitrogen for 15 min. Cyclic voltammetry was performed at 100 mV/sec from −0.3 to −1.3 V vs Ag/AgCl for 2 scans to create a terminal amine. Working carbon electrode was removed, rinsed thoroughly with UHP, and dried with compressed nitrogen.

IBP-3G-TEV Immobilization. 0.5 μg/mL Streptavidin-NHS ester was mixed with 1 mM ferricyanide in PBS. The reaction

https://doi.org/10.1021/acsomega.4c06481
ACS Omega 2024, 9, 39219−39231

was allowed to proceed overnight at 4 °C. The following day, electrodes were rinsed and placed in a 1 mg/mL IBP-3G-TEV solution for 1 h. The IBP-3G-TEV was solubilized in UHP with 3% ammonia.

Electrochemical Impedance Spectroscopy. Insulin was solubilized in 0.5 M HCl pH balanced to 7 with NaOH and stored at −20 °C in stocks at a 10 μM concentration. To achieve desired concentrations, the necessary stocks were thawed immediately prior to experimental use, and diluted using 1X PBS. Insulin was added to the electrochemical cell to achieve the desired concentration and allowed to equilibrate for 20 min. Electrochemical impedance spectroscopy was performed with an initial frequency of 10,000 Hz, final frequency of 0.1 Hz, 10 points/decade, and an initial delay of 250 s. An AC voltage of 10 mV rms with a DC offset of 0 V vs OCP was used.

Computational Analysis. Chain B from Protein Data Bank (PDB)[54] file 2x6m[55] was selected as the starting point for the predicted IBP structure on the sole basis of having the correct number of experimentally resolved amino acids (i.e., 6). UCSF Chimera[56] was used to mutate the peptide's residues to match the sequence of IBP (i.e., CVEEAS) using the 'swapaa' command and the dynameomics rotamer library.[57]

The MD simulation of IBP in explicit solvent was carried out using Nanoscale Molecular Dynamics (NAMD)[58] with the Chemistry at HARvard Molecular Mechanics 36 (CHARMM36) force field[59,60] the transferable intermolecular potential with 3 points (TIP3P) explicit water model,[61] and the isothermal−isobaric (NPT) ensemble. The QwikMD[62] plugin of Visual Molecular Dynamics (VMD)[63] was used to generate the simulation files. The simulation used a salt concentration of 0.15 mol/L of NaCl, was 2.5 ns long, and used a 2 fs time step with 2,000 minimization steps, 144,000 annealing steps, and 1,250,000 steps each for equilibration and simulation. Calculations took 5 h and 54 min to complete on a 3.00 GHz Intel Xeon Gold 6248R processor with 48 cores and 192 GB of available memory, which is a standard node on the Auburn University Easley Cluster. 1,000 IBP conformations were generated at evenly spaced time intervals from the simulation.

A clustering algorithm based upon previous work[64] was used to partition the MD-generated IBP conformations into groups of similar structures. Before clustering, the root mean squared deviations (RMSDs) of each unique pair of IBP conformations were calculated using their backbone atoms (i.e., N, Cα, and C). During this agglomerative, "bottom-up" clustering process, a representative IBP structure is selected as the model of each cluster. Model structure selection starts with identifying the worst (i.e., highest) RMSD value for each structure with any other member of the cluster. The structure selected as the cluster model is the one with the smallest worst RMSD, and this value is used as the score for the cluster. In other words, every member of a cluster has an RMSD no worse than the cluster score with the model structure of the cluster. Clustering began with each conformation as the sole member of a cluster. During each iteration, the pair of clusters yielding the lowest score when combined into a single cluster were grouped together. Clustering continued until no additional clusters with scores $\leq$1 Å could be created. The clustering process was repeated using all-atom, instead of backbone atom, RMSDs with a final cutoff of 1.5 Å.

Each of the 25 model structures identified by the clustering processes were docked to the structure of monomeric insulin found in PDB file 3i40[65] using ZDOCK,[47] which predicted ten conformations for each model structure for a total of 250 predicted IBP-insulin complexes. The predicted complexes were minimized using a strong harmonic backbone constraint with CHARMM36,[59,66] reminimized using an all atom energy minimization with Rosetta,[67] and their interface properties were analyzed with the Rosetta Interface Analyzer (RIA).[68] The use of constrained CHARMM energy minimizations followed by Rosetta all atom minimizations is consistent with our previous work.[69,70] It is our experience that CHARMM is able to resolve interface clashes better than other force fields while RIA provides comprehensive data about interfaces.

The two complexes that positioned IBP near the experimentally reported binding site on insulin and had the lowest predicted interaction energies were selected for MD analysis. The MD simulations used the same parameters as previously described, with the exception of being 100 ns in length, using 2,500,000 equilibration steps, using 50,000,000 simulation steps, and using the isothermal-isochoric (NVT) ensemble. 5000 conformations were saved from each simulation for analysis. The simulations took a few hours more than five and a half days to complete on a standard Easley Cluster node. The SH3-Ark1 complex in PDB file 2rpn[71] was selected as a control protein-peptide complex with an experimentally known structure. The control complex was run through a 100 ns MD simulation using identical parameters as the predicted IBP complexes, which took ~ 10.5 days on a standard Easley Cluster node. In each of the 5000 structures reported from each MD simulation, the minimum distances between the peptides and target proteins were calculated, along with all atom RMSD values. The NVT ensemble was used for these longer MD simulations to facilitate tracking the distance between IBP and insulin after dissociation, as they moved far apart and were observed crossing the periodic boundary conditions of the simulations.

ELISA. 50 μL of 10 μM insulin solubilized in 0.5 M 4% HCl, pH balanced with NaOH, and diluted to appropriate experimental concentrations with 1X PBS was added to all necessary wells of a high binding well plate and left at 4 °C overnight. The following day all wells were washed three times with ELISA wash buffer composed of 1% Tween-20 in PBS. 200 μL of commercial blocking buffer was then added to each well and allowed to incubate on the benchtop for 2 h.

IBP-3G-TEV and streptavidin were mixed in a centrifuge tube for 2 h. The wells were washed, and the IBP-streptavidin complex was added to all wells and allowed to incubate on a shaker for 2 h. Another wash was performed, and antistreptavidin antibody/HRP was added to all wells and allowed to incubate on a shaker for 2 h. A final wash was performed, and tetramethylbenzidine was added to each well and allowed to react for 15 min. 0.1 M sulfuric acid was added to all wells to stop the reaction, and a plate reader at 650 nm was used to determine initial baseline measurements.

Negative controls were created by using commercial blocking buffer in place of insulin at the initial stage. A positive control was created by replacing insulin with antistreptavidin/HRP at the initial stage. All ELISA experiments were repeated in triplicate.

Isothermal Titration Calorimetry (ITC). ITC experiments were performed using a TA instructions Affinity ITC. IBP and insulin were dissolved in fresh, identical buffer solutions containing 20 mM HEPES pH 7.5, 100 mM NaCl, and 2 mM EDTA. The reference cell was freshly washed and

https://doi.org/10.1021/acsomega.4c06481
ACS Omega 2024, 9, 39219−39231

filled with milliQ water and matched the initial sample cell volume. Baseline control runs were completed with each experimental run. Control runs used a syringe filled with the buffer solution used to titrate the samples instead of using IBP solution. All experiments were performed at 25 °C, stir rate of 125 rpm, with injection volumes of 2.5 μL and 90−120 s of equilibration time between injections. The first study to identify possible binding characteristics used an initial concentration ratio of $8_{Syringe}$:1_{Cell} with the syringe containing 20 μM IBP and the sample cell containing 2.5 μM insulin. The second study adjusted the initial ratio to $5_{Syringe}$:1_{Cell} with 1 mM IBP in the syringe and 200 μM insulin in the sample cell. Data were analyzed and figures were generated using the manufacturer's NanoAnalyze software.

■ ASSOCIATED CONTENT

Data Availability Statement

The data underlying this study are openly available in Dryad at doi:10.5061/dryad.bzkh189jq.

■ AUTHOR INFORMATION

Corresponding Author

Robert J. Pantazes − *Department of Chemical Engineering, Auburn University, Auburn, Alabama 36849, United States;* orcid.org/0000-0002-0994-007X; Email: rjp0029@auburn.edu

Authors

Katherine Austin − *Department of Chemical Engineering and Bioengineering, University of New Hampshire, Durham, New Hampshire 03824, United States*

Jazmine A. Torres − *Department of Chemical Engineering, Auburn University, Auburn, Alabama 36849, United States*

Jeffery D. V. Waters − *School of Molecular and Physical Sciences, University of New England, Biddeford, Maine 04005, United States;* orcid.org/0009-0009-9054-7846

Eva Rose M. Balog − *School of Molecular and Physical Sciences, University of New England, Biddeford, Maine 04005, United States;* orcid.org/0000-0001-6792-6914

Jeffrey M. Halpern − *Department of Chemical Engineering and Bioengineering, University of New Hampshire, Durham, New Hampshire 03824, United States;* orcid.org/0000-0003-0814-1986

Complete contact information is available at: https://pubs.acs.org/10.1021/acsomega.4c06481

Author Contributions

‖K.A., J.A.T., and J.D.V.W. contributed equally to this work.

Notes

The authors declare no competing financial interest.

■ ACKNOWLEDGMENTS

This work was funded by the NSF EPSCoR RII Track-2 Award 2119237. It was completed in part using the Auburn University Easley Cluster. NAMD was developed by the Theoretical and Computational Biophysics Group in the Beckman Institute for Advanced Science and Technology at the University of Illinois at Urbana−Champaign. The authors would like to acknowledge the assistance of Mariah Arral in development of the ELISA procedure and the Furst lab at MIT for assistance with the NHS-ester synthesis and aminophenol streptavidin protocol development. The authors are grateful to Eleenah Sanders for assistance in ITC figure preparation.

■ REFERENCES

(1) Trier, N.; Hansen, P.; Houen, G. Peptides, Antibodies, Peptide Antibodies and More. *Int. J. Molecular Sci.* **2019**, *20* (24), 6289.

(2) Zhao, X.; An, X.; Yang, C.; Sun, W.; Ji, H.; Lian, F. The crucial role and mechanism of insulin resistance in metabolic disease. *Front. Endocrinol.* **2023**, *14*, 1149239.

(3) Vargas, E.; Nandhakumar, P.; Ding, S.; Saha, T.; Wang, J. Insulin detection in diabetes mellitus: challenges and new prospects. *Nat. Rev. Endocrinol.* **2023**, *19* (8), 487−495.

(4) Lin, R.; Brown, F.; James, S.; Jones, J.; Ekinci, E. Continuous glucose monitoring: A review of the evidence in type 1 and 2 diabetes mellitus. *Diabetic Med.* **2021**, *38* (5), No. e14528.

(5) Psoma, S. D.; Kanthou, C. Wearable Insulin Biosensors for Diabetes Management: Advances and Challenges. *Biosensors* **2023**, *13* (7), 719.

(6) Fact Sheet: Biden-Harris Administration's Actions to Advance American Biotechnology and Biomanufacturing. Policy, O. o. S. a. T., Ed. Internet, 2024.

(7) Lian, X.; Palecek, S. P. Biomanufacturing Human Pluripotent Stem Cells for Therapeutic Applications. In *Advances in Stem Cell Research*; Baharvand, H.; Aghdami, N., Eds.; Humana Press: Totowa, NJ, 2012; pp 29−48.

(8) Adamson, L.; Walum, E. Insulin and IGF-1 Mediated Inhibition of Apoptosis in CHO Cells Grown in Suspension in a Protein-free Medium. *Alternatives Laboratory Animals* **2007**, *35* (3), 349−352.

(9) Morris, A. E.; Schmid, J. Effects of Insulin and LongR3 on Serum-Free Chinese Hamster Ovary Cell Cultures Expressing Two Recombinant Proteins. *Biotechnol. Prog.* **2000**, *16* (5), 693−697.

(10) O'Flaherty, R.; Bergin, A.; Flampouri, E.; Mota, L. M.; Obaidi, I.; Quigley, A.; Xie, Y.; Butler, M. Mammalian cell culture for production of recombinant proteins: A review of the critical steps in their biomanufacturing. *Biotechnol. Adv.* **2020**, *43*, No. 107552.

(11) Iworima, D. G.; Rieck, S.; Kieffer, T. J. Process Parameter Development for the Scaled Generation of Stem Cell-Derived Pancreatic Endocrine Cells. *Stem Cells Translat. Med.* **2021**, *10* (11), 1459−1469.

(12) McCorry, M. C.; Reardon, K. F.; Black, M.; Williams, C.; Babakhanova, G.; Halpern, J. M.; Sarkar, S.; Swami, N. S.; Mirica, K. A.; Boermeester, S.; Underhill, A. Sensor technologies for quality control in engineered tissue manufacturing. *Biofabrication* **2023**, *15* (1), No. 012001.

(13) Amouzadeh Tabrizi, M.; Shamsipur, M.; Saber, R.; Sarkar, S.; Besharati, M. An electrochemical aptamer-based assay for femtomolar determination of insulin using a screen printed electrode modified with mesoporous carbon and 1,3,6,8-pyrenetetrasulfonate. *Microchimica Acta* **2018**, *185* (1), 59.

(14) Luong, A.-D.; Roy, I.; Malhotra, B. D.; Luong, J. H. T. Analytical and biosensing platforms for insulin: A review. *Sensors Actuators Rep.* **2021**, *3*, No. 100028.

(15) Yoshida, W.; Mochizuki, E.; Takase, M.; Hasegawa, H.; Morita, Y.; Yamazaki, H.; Sode, K.; Ikebukuro, K. Selection of DNA aptamers against insulin and construction of an aptameric enzyme subunit for insulin sensing. *Biosens. Bioelect.* **2009**, *24* (5), 1116−1120.

(16) Taghdisi, S. M.; Danesh, N. M.; Lavaee, P.; Sarreshtehdar Emrani, A.; Ramezani, M.; Abnous, K. Aptamer Biosensor for Selective and Rapid Determination of Insulin. *Anal. Lett.* **2015**, *48* (4), 672−681.

(17) Gerasimov, J. Y.; Schaefer, C. S.; Yang, W.; Grout, R. L.; Lai, R. Y. Development of an electrochemical insulin sensor based on the insulin-linked polymorphicregion. *Biosens. Bioelect.* **2013**, *42*, 62−68.

(18) Wu, Y.; Midinov, B.; White, R. J. Electrochemical Aptamer-Based Sensor for Real-Time Monitoring of Insulin. *ACS Sens.* **2019**, *4* (2), 498−503.

(19) Kartal, F.; Çimen, D.; Bereli, N.; Denizli, A. Molecularly imprinted polymer based quartz crystal microbalance sensor for the clinical detection of insulin. *Mater. Sci. Eng.: C* **2019**, *97*, 730−737.

(20) Garcia Cruz, A.; Haq, I.; Cowen, T.; Di Masi, S.; Trivedi, S.; Alanazi, K.; Piletska, E.; Mujahid, A.; Piletsky, S. A. Design and fabrication of a smart sensor using in silico epitope mapping and electro-responsive imprinted polymer nanoparticles for determination of insulin levels in human plasma. *Biosens. Bioelect.* **2020**, *169*, No. 112536.
(21) Zidarič, T.; Majer, D.; Maver, T.; Finšgar, M.; Maver, U. The development of an electropolymerized, molecularly imprinted polymer (MIP) sensor for insulin determination using single-drop analysis. *Analyst* **2023**, *148* (5), 1102−1115.
(22) Xu, M.; Luo, X.; Davis, J. J. The label free picomolar detection of insulin in blood serum. *Biosens. Bioelect.* **2013**, *39* (1), 21−25.
(23) Malkoc, A.; Probst, D.; Lin, C.; Khanwalker, M.; Beck, C.; Cook, C. B.; La Belle, J. T. Enhancing Glycemic Control via Detection of Insulin Using Electrochemical Impedance Spectroscopy. *J. Diabetes Sci. Technol.* **2017**, *11* (5), 930−935.
(24) Rodríguez-Gutiérrez, R.; Cámara-Lemarroy, C. R.; Quintanilla-Flores, D. L.; González-Moreno, E. I.; González-Chávez, J. M.; Lavalle-González, F. J.; González-González, J. G.; Caballero, A. E. Severe Ketoacidosis (pH ≤ 6.9) in Type 2 Diabetes: More Frequent and Less Ominous Than Previously Thought. *BioMed Res. Int.* **2015**, *2015* (1), No. 134780.
(25) Wilson, G. S.; Gifford, R. Biosensors for real-time in vivo measurements. *Biosens. Bioelect.* **2005**, *20* (12), 2388−2403.
(26) Wang, H.; Nakata, E.; Hamachi, I. Recent Progress in Strategies for the Creation of Protein-Based Fluorescent Biosensors. *ChemBioChem* **2009**, *10* (16), 2560−2577.
(27) Morales, M. A.; Halpern, J. M. Guide to Selecting a Biorecognition Element for Biosensors. *Bioconjugate Chem.* **2018**, *29* (10), 3231−3239.
(28) Khanwalker, M.; Fujita, R.; Lee, J.; Wilson, E.; Ito, K.; Asano, R.; Ikebukuro, K.; LaBelle, J.; Sode, K. Development of a POCT type insulin sensor employing anti-insulin single chain variable fragment based on faradaic electrochemical impedance spectroscopy under single frequency measurement. *Biosens. Bioelect.* **2022**, *200*, No. 113901.
(29) Peltomaa, R.; Benito-Peña, E.; Barderas, R.; Moreno-Bondi, M. C. Phage Display in the Quest for New Selective Recognition Elements for Biosensors. *ACS Omega* **2019**, *4* (7), 11569−11580.
(30) Kuang, Z.; Kim, S. N.; Crookes-Goodson, W. J.; Farmer, B. L.; Naik, R. R. Biomimetic Chemosensor: Designing Peptide Recognition Elements for Surface Functionalization of Carbon Nanotube Field Effect Transistors. *ACS Nano* **2010**, *4* (1), 452−458.
(31) Qiao, Z.; Fu, Y.; Lei, C.; Li, Y. Advances in antimicrobial peptides-based biosensing methods for detection of foodborne pathogens: A review. *Food Control* **2020**, *112*, No. 107116.
(32) Knutson, V. P. Insulin-binding peptide. Design and characterization. *J. Biol. Chem.* **1988**, *263* (28), 14146−14151.
(33) Root-Bernstein, R. S.; Holsworth, D. D. Antisense Peptides: A Critical Mini-Review. *J. Theor. Biol.* **1998**, *190* (2), 107−119.
(34) Blalock, J. E.; Smith, E. M. Hydropathic anti-complementarity of amino acids based on the genetic code. *Biochem. Biophys. Res. Commun.* **1984**, *121* (1), 203−207.
(35) Stambuk, N.; Konjevoda, P.; Boban-Blagaić, A.; Pokrić, B. Molecular Recognition Theory of the complementary (antisense) peptide interactions. *Theory Biosci.* **2005**, *123* (4), 265−275.
(36) Blalock, J. E. Genetic origins of protein shape and interaction rules. *Nat. Med.* **1995**, *1* (9), 876−878.
(37) Blalock, J. E.; Bost, K. L. Binding of peptides that are specified by complementary RNAs. *Biochem. J.* **1986**, *234* (3), 679−683.
(38) Chaiken, I. Interactions and uses of antisense peptides in affinity technology. *J. Chromatogr. A* **1992**, *597* (1), 29−36.
(39) Tropsha, A.; Kizer, J. S.; Chaiken, I. M. Making sense from antisense: A review of experimental data and developing ideas on sense−antisense peptide recognition. *J. Mol. Recognit.* **1992**, *5* (2), 43−54.
(40) Bisker, G.; Bakh, N. A.; Lee, M. A.; Ahn, J.; Park, M.; O'Connell, E. B.; Iverson, N. M.; Strano, M. S. Insulin Detection Using a Corona Phase Molecular Recognition Site on Single-Walled Carbon Nanotubes. *ACS Sens.* **2018**, *3* (2), 367−377.
(41) Eriksson, M.; Litwak, S. A.; Yun, Y.; Stanley, W. J.; Thorn, P.; Ahlgren, U.; Gurzov, E. N. Insulin-Binding Peptide Probes Provide a Novel Strategy for Pancreatic β-Cell Imaging. *Mol. Pharmaceutics* **2021**, *18* (12), 4428−4436.
(42) Panahi, Z.; Ren, T.; Halpern, J. M. Nanostructured Cyclodextrin-Mediated Surface for Capacitive Determination of Cortisol in Multiple Biofluids. *ACS Appl. Mater. Interfaces* **2022**, *14* (37), 42374−42387.
(43) Magar, H. S.; Hassan, R. Y. A.; Mulchandani, A. Electrochemical Impedance Spectroscopy (EIS): Principles, Construction, and Biosensing Applications. *Sensors* **2021**, *21*, 6578.
(44) Helali, S.; Fredj, H. B.; Cherif, K.; Abdelghani, A.; Martelet, C.; Jaffrezic-Renault, N. Surface plasmon resonance and impedance spectroscopy on gold electrode for biosensor application. *Mater. Sci. Eng.: C* **2008**, *28* (5), 588−593.
(45) Sheen, H.-J.; Panigrahi, B.; Kuo, T.-R.; Hsu, W.-C.; Chung, P.-S.; Xie, Q.-Z.; Lin, C.-Y.; Chang, Y.-S.; Lin, C.-T.; Fan, Y.-J. Electrochemical biosensor with electrokinetics-assisted molecular trapping for enhancing C-reactive protein detection. *Biosens. Bioelect.* **2022**, *210*, No. 114338.
(46) Panahi, Z.; Merrill, M. A.; Halpern, J. M. Reusable Cyclodextrin-Based Electrochemical Platform for Detection of trans-Resveratrol. *ACS Appl. Polym. Mater.* **2020**, *2* (11), 5086−5093.
(47) Pierce, B. G.; Wiehe, K.; Hwang, H.; Kim, B.-H.; Vreven, T.; Weng, Z. ZDOCK server: interactive docking prediction of protein−protein complexes and symmetric multimers. *Bioinformatics* **2014**, *30* (12), 1771−1773.
(48) Baek, M.; DiMaio, F.; Anishchenko, I.; Dauparas, J.; Ovchinnikov, S.; Lee, G. R.; Wang, J.; Cong, Q.; Kinch, L. N.; Schaeffer, R. D.; Millán, C.; Park, H.; Adams, C.; Glassman, C. R.; DeGiovanni, A.; Pereira, J. H.; Rodrigues, A. V.; van Dijk, A. A.; Ebrecht, A. C.; Opperman, D. J.; Sagmeister, T.; Buhlheller, C.; Pavkov-Keller, T.; Rathinaswamy, M. K.; Dalwadi, U.; Yip, C. K.; Burke, J. E.; Garcia, K. C.; Grishin, N. V.; Adams, P. D.; Read, R. J.; Baker, D. Accurate prediction of protein structures and interactions using a three-track neural network. *Science* **2021**, *373* (6557), 871−876.
(49) Jumper, J.; Evans, R.; Pritzel, A.; Green, T.; Figurnov, M.; Ronneberger, O.; Tunyasuvunakool, K.; Bates, R.; Žídek, A.; Potapenko, A.; Bridgland, A.; Meyer, C.; Kohl, S. A. A.; Ballard, A. J.; Cowie, A.; Romera-Paredes, B.; Nikolov, S.; Jain, R.; Adler, J.; Back, T.; Petersen, S.; Reiman, D.; Clancy, E.; Zielinski, M.; Steinegger, M.; Pacholska, M.; Berghammer, T.; Bodenstein, S.; Silver, D.; Vinyals, O.; Senior, A. W.; Kavukcuoglu, K.; Kohli, P.; Hassabis, D. Highly accurate protein structure prediction with AlphaFold. *Nature* **2021**, *596* (7873), 583−589.
(50) Krainer, G.; Broecker, J.; Vargas, C.; Fanghänel, J.; Keller, S. Quantifying High-Affinity Binding of Hydrophobic Ligands by Isothermal Titration Calorimetry. *Anal. Chem.* **2012**, *84* (24), 10715−10722.
(51) Ge, X.; Chen, L.; Li, D.; Liu, R.; Ge, G. Estimation of non-constant variance in isothermal titration calorimetry using an ITC measurement model. *PLoS One* **2020**, *15* (12), No. e0244739.
(52) Krainer, G.; Keller, S. Single-experiment displacement assay for quantifying high-affinity binding by isothermal titration calorimetry. *Methods* **2015**, *76*, 116−123.
(53) *Thermo Scientific Avidin-Biotin Technical Handbook*; Thermo Fisher Scientific Inc, 2009.
(54) Berman, H. M.; Westbrook, J.; Feng, Z.; Gilliland, G.; Bhat, T. N.; Weissig, H.; Shindyalov, I. N.; Bourne, P. E. The Protein Data Bank. *Nucleic Acids Res.* **2000**, *28* (1), 235−242.
(55) De Genst, E. J.; Guilliams, T.; Wellens, J.; O'Day, E. M.; Waudby, C. A.; Meehan, S.; Dumoulin, M.; Hsu, S.-T. D.; Cremades, N.; Verschueren, K. H. G.; Pardon, E.; Wyns, L.; Steyaert, J.; Christodoulou, J.; Dobson, C. M. Structure and Properties of a Complex of α-Synuclein and a Single-Domain Camelid Antibody. *J. Mol. Biol.* **2010**, *402* (2), 326−343.

https://doi.org/10.1021/acsomega.4c06481
ACS Omega 2024, 9, 39219−39231

(56) Pettersen, E. F.; Goddard, T. D.; Huang, C. C.; Couch, G. S.; Greenblatt, D. M.; Meng, E. C.; Ferrin, T. E. UCSF Chimera—A Visualization System for Exploratory Research and Analysis. *J. Comput. Chem.* **2004**, *25*, 1605−1612.
(57) Scouras, A. D.; Daggett, V. The dynameomics rotamer library: Amino acid side chain conformations and dynamics from comprehensive molecular dynamics simulations in water. *Protein Sci.* **2011**, *20* (2), 341−352.
(58) Phillips, J. C.; Braun, R.; Wang, W.; Gumbart, J.; Tajkhorshid, E.; Villa, E.; Chipot, C.; Skeel, R. D.; Kalé, L.; Schulten, K. Scalable molecular dynamics with NAMD. *J. Comput. Chem.* **2005**, *26* (16), 1781−1802.
(59) Brooks, B. R.; Brooks, C. L., 3rd; Mackerell, A. D., Jr; Nilsson, L.; Petrella, R. J.; Roux, B.; Won, Y.; Archontis, G.; Bartels, C.; Boresch, S.; Caflisch, A.; Caves, L.; Cui, Q.; Dinner, A. R.; Feig, M.; Fischer, S.; Gao, J.; Hodoscek, M.; Im, W.; Kuczera, K.; Lazaridis, T.; Ma, J.; Ovchinnikov, V.; Paci, E.; Pastor, R. W.; Post, C. B.; Pu, J. Z.; Schaefer, M.; Tidor, B.; Venable, R. M.; Woodcock, H. L.; Wu, X.; Yang, W.; York, D. M.; Karplus, M. CHARMM: the biomolecular simulation program. *J. Comput. Chem.* **2009**, *30* (10), 1545−1614.
(60) Lee, J.; Cheng, X.; Swails, J. M.; Yeom, M. S.; Eastman, P. K.; Lemkul, J. A.; Wei, S.; Buckner, J.; Jeong, J. C.; Qi, Y.; Jo, S.; Pande, V. S.; Case, D. A.; Brooks, C. L., III; MacKerell, A. D., Jr.; Klauda, J. B.; Im, W. CHARMM-GUI Input Generator for NAMD, GROMACS, AMBER, OpenMM, and CHARMM/OpenMM Simulations Using the CHARMM36 Additive Force Field. *J. Chem. Theory Comput.* **2016**, *12* (1), 405−413.
(61) Jorgensen, W. L.; Chandrasekhar, J.; Madura, J. D.; Impey, R. W.; Klein, M. L. Comparison of simple potential functions for simulating liquid water. *J. Chem. Phys.* **1983**, *79* (2), 926−935.
(62) Ribeiro, J. V.; Bernardi, R. C.; Rudack, T.; Stone, J. E.; Phillips, J. C.; Freddolino, P. L.; Schulten, K. QwikMD — Integrative Molecular Dynamics Toolkit for Novices and Experts. *Sci. Rep.* **2016**, *6* (1), No. 26536.
(63) Humphrey, W.; Dalke, A.; Schulten, K. VMD: Visual molecular dynamics. *J. Mol. Graphics* **1996**, *14* (1), 33−38.
(64) Pantazes, R. J.; Maranas, C. D. OptCDR: A general computational method for the design of antibody complementarity determining regions for targeted epitope binding. *Protein Eng., Design Selection* **2010**, *23* (11), 849−858.
(65) Timofeev, V. I.; Chuprov-Netochin, R. N.; Samigina, V. R.; Bezuglov, V. V.; Miroshnikov, K. A.; Kuranova, I. P. X-ray investigation of gene-engineered human insulin crystallized from a solution containing polysialic acid. *Acta Crystallog. F Struct. Biol. Crystallizat. Commun.* **2010**, *66* (3), 259−263.
(66) Brooks, B. R.; Bruccoleri, R. E.; Olafson, B. D.; States, D. J.; Swaminathan, S.; Karplus, M. CHARMM: A program for macromolecular energy, minimization, and dynamics calculations. *J. Comput. Chem.* **1983**, *4* (2), 187−217.
(67) Alford, R. F.; Leaver-Fay, A.; Jeliazkov, J. R.; O'Meara, M. J.; DiMaio, F. P.; Park, H.; Shapovalov, M. V.; Renfrew, P. D.; Mulligan, V. K.; Kappel, K.; Labonte, J. W.; Pacella, M. S.; Bonneau, R.; Bradley, P.; Dunbrack, R. L.; Das, R.; Baker, D.; Kuhlman, B.; Kortemme, T.; Gray, J. J. The Rosetta All-Atom Energy Function for Macromolecular Modeling and Design. *J. Chem. Theory Comput.* **2017**, *13* (6), 3031−3048.
(68) Leaver-Fay, A.; Tyka, M.; Lewis, S. M.; Lange, O. F.; Thompson, J.; Jacak, R.; Kaufman, K. W.; Renfrew, P. D.; Smith, C. A.; Sheffler, W.; Davis, I. W.; Cooper, S.; Treuille, A.; Mandell, D. J.; Richter, F.; Ban, Y.-E. A.; Fleishman, S. J.; Corn, J. E.; Kim, D. E.; Lyskov, S.; Berrondo, M.; Mentzer, S.; Popović, Z.; Havranek, J. J.; Karanicolas, J.; Das, R.; Meiler, J.; Kortemme, T.; Gray, J. J.; Kuhlman, B.; Baker, D.; Bradley, P. Rosetta3: An Object-Oriented Software Suite for the Simulation and Design of Macromolecules. In *Methods Enzymol.*; Johnson, M. L.; Brand, L., Eds.; Academic Press, 2011; Vol. *487*, Chapter 19, pp 545−574.
(69) Chauhan, V. M.; Pantazes, R. J. Analysis of conformational stability of interacting residues in protein binding interfaces. *Protein Eng., Design Select.* **2023**, *36*, No. gzad016.
(70) Chauhan, V. M.; Pantazes, R. J. MutDock: A computational docking approach for fixed-backbone protein scaffold design. *Front. Molecular Biosci.* **2022**, *9*, 933400.
(71) Stollar, E. J.; Garcia, B.; Chong, P. A.; Rath, A.; Lin, H.; Forman-Kay, J. D.; Davidson, A. R. Structural, Functional, and Bioinformatic Studies Demonstrate the Crucial Role of an Extended Peptide Binding Site for the SH3 Domain of Yeast Abp1p*. *J. Biol. Chem.* **2009**, *284* (39), 26918−26927.

NOTE ADDED AFTER ASAP PUBLICATION

In the **Computational Analysis** paragraph the PDB code 2x6m was corrected on September 6, 2024.

https://doi.org/10.1021/acsomega.4c06481
ACS Omega 2024, 9, 39219−39231